UNIVERSIDAD INDUSTRIAL DE SANTANDER
Escuela de Ingenierías Eléctrica, Electrónica y de Telecomunicaciones

Design of a Current Meter for Measurement Under Normal Operation and Deep Sleep Conditions on a Microcontroller

Presented To:
Jaime Guillermo Barrero Pérez

By:
Jorge Walter Sanchez Fonce
Santiago Castro Rondón

Universidad Industrial de Santander
Escuela de Ingenierías Eléctrica, Electrónica y de Telecomunicaciones
Bucaramanga - 2025

Contents

List of Figures

List of Tables

1 Introduction

With the growing demand for energy-efficient embedded systems, the ability to accurately measure current consumption across different operating states of a microcontroller has become increasingly important. Many battery-operated devices, such as those based on the ESP32, rely on sleep and active cycles to prolong operational life. Consequently, monitoring current in both active and deep sleep modes is essential for evaluating and optimizing energy consumption.
This project addresses that need by designing a battery-powered electronic circuit capable of measuring the current drawn by a microcontroller as it alternates periodically between its normal and deep sleep modes. Furthermore, to facilitate real-time monitoring and data logging, the measured current is wirelessly transmitted to a computer or mobile device. The complete solution includes the design of the printed circuit board (PCB), as well as a control interface that allows both manual and automatic switching between current measurement ranges.

2 Problem Definition

In embedded system design, the ability to monitor and optimize power consumption is critical, particularly for battery operated devices where energy efficiency directly impacts device longevity and reliability. Microcontrollers such as the ESP32 often operate in multiple power modes, including a high consumption active mode and a low consumption deep sleep mode. Measuring the current accurately across these states is essential for characterizing system performance and making informed design decisions.
The primary challenge lies in developing a circuit that can measure a wide range of currents—spanning from the microampere level during sleep to the milliampere level during active operation without introducing significant voltage drop or measurement noise. Moreover, since the microcontroller changes periodically between modes (every 10 seconds, in this case), the current sensing solution must be fast and adaptive enough to respond to these rapid changes.
To meet these demands, this project aims to design a battery-powered current measurement system capable of operating in both manual and automatic modes. In manual mode, the user selects the measurement range, while in automatic mode, the system detects and adjusts to the appropriate range based on the observed current. The output voltage of the measurement circuit must not exceed 1000 mV in any condition, preserving compatibility with downstream processing and data acquisition systems.
In addition to measurement accuracy and dynamic range, the solution must support wireless communication to transmit the measured data to a computer or mobile device, enabling real time monitoring. Finally, the selection of components and the overall PCB design must take into account factors such as size, power consumption, and cost, to ensure the system is practical for deployment in real world low power embedded applications.

3 Design Choices

The proposed circuit for current measurements consists of an analog block that reads and amplifies the voltage signal across the shunt resistor for further processing, and a digital block that manages the switching logic of the PMOS transistors. These transistors determine the current measurement range and whether the device operates in automatic or manual mode.
The following section explains the criteria used to select each component in the circuit [2]. Each component was carefully and individually chosen based on its specific role within the design.

3.1 Operational Amplifiers

To amplify the voltage across the shunt resistors, two amplification stages are connected using operational amplifiers with a feedback loop that sets the voltage gain of each stage, resulting in a total gain of 100 V/V.

The selected MAX4239 amplifiers, as shown in Table 1 feature ultra-high precision and low noise susceptibility, making them capable of achieving an almost zero DC offset through the use of autocorrelating zeroing techniques to compensate for input offset. These characteristics make them ideal for this application, where extremely low and sensitive voltage levels are involved, and any offset cannot be tolerated.

Table 1: MAX4239 Offset Voltage Specifications

Temperature Range	Offset Voltage (Max)	Units
$+25°C$	2.0	μV
$-40°C$ to $+85°C$	2.5	μV
$-40°C$ to $+125°C$	3.5	μV

Table 2: Comparison of Operational Amplifiers Based on Offset Voltage and Cost

Op-Amp	Typical Offset Voltage (μV)	Maximum Offset Voltage (μV)	Price (USD)
MAX4239	0.1	3.5	4.56
TLV333	2	15	1.41
MCP6V01	-	2	5.64
ADA4530-1	9	50	31.09
AD8629	1	5	14.2

When comparing the key characteristics and prices of high-precision operational amplifiers, two main candidates emerged: the MAX4239 and the TLV333. However, the MAX4239 was chosen because it has been characterized by LowPowerLabs during the development of the Current Ranger, ensuring greater reliability and predictability. Additionally, the TLV333 is not characterized for typical operating conditions, making it less suitable for this application. Moreover, the price difference between the two is not significant.

3.2 Switching Transistors

Since the system operates in multiple modes, a switching logic was implemented using Si7141DP PMOS transistors, which are controlled by digital outputs from the ESP32. The main criterion for selecting these transistors was their low on-resistance, as the goal was to approximate the behavior of an ideal switch, minimizing voltage drop across the switching element. The initial set of transistors

considered is shown in the following table:

Table 3: Comparison of PMOS Transistors with Low On-Resistance

Transistor	V_{DS} (V)	V_{GS} (V)	$R_{DS(on)}$ (mΩ)	I_D (A)	Price (USD)
Si7141DP	-20	-10	1.9	60	2.51
Si7157DP	-20	-10	1.6	60	1.68
SiRA99DP	-30	-10	1.7	60	1.50
SiSS05DN	-30	-10	3.5	20	0.90

3.3 Clamp Transistors

The MMBT6429 (PNP) and MMBT6428 (NPN) transistors were selected as clamps in the Current Ranger due to their ultra-low leakage current (<1 nA), which is crucial to prevent distortion in microampere-level measurements, and their fast transient response (low capacitance and 10 ns switching time). Additionally, their SOT-23 package optimizes PCB space and minimizes parasitic effects. Their balance between precision, protection, and cost makes them superior to alternatives such as the 2N3904, which exhibits higher leakage current. This ensures that they do not degrade the signal across the 0.01Ω shunt resistor or introduce significant errors in any measurement range.

3.4 Low Pass Filter Transistor

The BC550 was selected for the low-pass filter due to its superior low-noise performance, as indicated in Table 4. Compared to other alternatives such as the 2N3904 and 2N2222, which exhibit medium noise levels, the BC550 ensures minimal signal distortion, making it ideal for precision analog applications. Additionally, its high transition frequency (300 MHz) provides sufficient bandwidth while maintaining stable operation. Given these advantages and its comparable price to other options, the BC550 is the most suitable choice for this design.

Table 4: Comparison of NPN Transistors for a Low-Pass Filter Application

Model	Low Noise	Transition Frequency (MHz)	Price (USD)
BC550	Yes	300	0.05
BC547	Yes	300	0.04
2N3904	Medium	250	0.07
2SC1815	Yes	80	0.2
2N2222	Medium	250	0.35

The following figure demonstrates the importance of incorporating the low-pass filter, showing that the signal can be identified with greater precision by effectively reducing high-frequency noise and unwanted fluctuations. This improvement enhances measurement accuracy and ensures more stable readings in the system.

3.5 Analog to Digital Converter

The ESP32's internal ADC was immediately discarded for this design due to its non-idealities, including poor linearity and accuracy, high noise levels, offset and gain errors, as well as high input

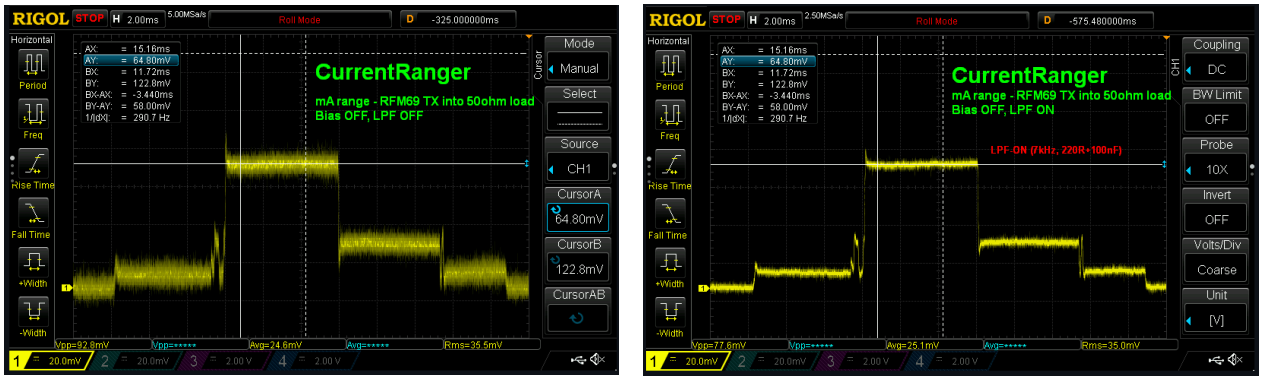

Figure 1: Comparison of signal quality with LPF OFF vs. LPF ON [1].

impedance and slow response. These limitations are critical in an application where the system must accurately respond to very small currents while maintaining moderate sensitivity within these ranges.

The LowPowerLabs Current Ranger utilizes the ADC of the ATSAMD21G18 microcontroller, which provides a reference point for evaluating key criteria such as ADC resolution and sampling rate, as shown in the following table.

Table 5: Comparison of ADCs

ADC Model	Resolution (bits)	Sampling Rate (kSPS)	Price (USD)
ADS8320EB/2K5	16	100	12.69
ADS1242IPWT-1	24	4	11.61
SAMD21 ADC	12	350	NA

Both ADCs exhibit significantly good characteristics compared to the one in the SAMD21. In fact, either could be used for this application due to their high precision. However, the ADS1242IPWT-1 was chosen. Despite its relatively low sampling rate, its high resolution makes it optimal for this environment, where extremely low voltages must be measured. Additionally, since the system does not handle high-speed signals, the selected sampling rate does not pose a limitation.

3.6 Microcontroller

Among the families of microcontrollers evaluated for managing the circuit's digital logic and communication with the web interface, the SAMD21, Raspberry Pi, ESP32, and Arduino were considered. However, after a thorough assessment, the Raspberry Pi was deemed excessive for the intended application, as its computational power far exceeds the system's requirements.

Conversely, the SAMD21 was ruled out due to its lack of an integrated Wi-Fi module, which is essential for the required web communication protocol. Additionally, in the original Current Ranger design, the SAMD21 was responsible for several functions that are not necessary in this implementation, further reducing its suitability.

Ultimately, the ESP32 was chosen over the Arduino due to its higher clock speed, larger RAM capacity, and built-in Wi-Fi connectivity, making it a more efficient and versatile solution for the given application.

Table 6: Comparison of Selected Microcontrollers

Device	Clock (MHz)	RAM	Flash	Wi-Fi	Power
ESP32	240	520 KB	4 MB	Yes	Low
Arduino Uno	16	2 KB	32 KB	No	Low
Arduino Mega	16	8 KB	256 KB	No	Low
Raspberry Pi 4	1500	2GB+	microSD	Yes	High
SAMD21	48	32 KB	256 KB	No	Very Low

Once the ESP32 family was selected, a module from the ESP32 Series was chosen due to its integrated Wi-Fi and Bluetooth connectivity, high processing power (up to 240 MHz dual-core architecture), and low power consumption in sleep mode (<5 µA). These features make it particularly suitable for the Current Ranger application, ensuring reliable wireless communication while maintaining energy efficiency. Additionally, its extensive peripheral support, including an SPI interface allows seamless integration with the external ADC and other essential components of the system.

The first modules to be discarded were those labeled as NRFND (Not Recommended for New Designs) and EOL (End of Life), as using them in a new design could compromise long-term availability and technical support. This led to the selection of the ESP32-WROOM-32E due to its assured availability, full certification, optimized performance, and improved energy efficiency compared to previous versions.
Besides, this module features 4 MB of SPI Flash memory, an integrated antenna, and support for 2.4 GHz Wi-Fi and Bluetooth LE, making it ideal for the Current Ranger application, where stable wireless communication and low power consumption are key factors.

3.7 ADC Oscillator

The selected ADC is the ADS1242IPWT-1, which does not have an internal clock signal required for proper data conversion. Therefore, it is necessary to generate this clock signal externally. Two options are recommended: using a crystal oscillator in conjunction with the clock generator already present within the ADC to generate the required clock signal, or employing a signal generator to produce the desired signal.
The decision was made to choose a 4.096 MHz crystal oscillator, which was considered the best option due to its small size, cost-effectiveness, and ease of implementation on the PCB. For this clock, extremely high precision was not required, as the clock generator within the ADC compensates for errors caused by the external clock. It is also important to clarify that the drawback of using a crystal oscillator is the need to implement it with two capacitors, which takes up additional space on the breadboard. However, it was not believed that this would have a significant impact. The selected reference was the ABLS2, which has the following characteristics:

Table 7: Crystal Oscillator ABLS2 Specifications

Parameters	**Minimum**	**Typical**	**Maximum**	**Units**
Frequency Range	3.57	-	24.00	MHz
Operating Temperature	0	-	+70	°C
Load Capacitance (CL)	-	18	-	pF
Drive Level	100	-	1000	µW
Frequency Stability	-50	-	+50	ppm

Additionally, the two 18 pF capacitors required for the proper functioning of the oscillator are included.

3.8 Battery

The chosen battery is the XINJ 102540, which has a nominal voltage of 3.7V, a charge current of 1A, a capacity of 1300mAh, and 4.81mWh. The main specifications considered when selecting the battery were the charge current and its size, as the device, being small, could not have an excessively large battery. Additionally, it was essential that the battery be rechargeable. A higher-capacity battery was discarded because, although it would have ensured longer device runtime, it would have been too large compared to the size of the PCB. Furthermore, as a current meter, the device would not be in prolonged use, so with this battery, 2 hours of daily use for a week can be ensured.

Table 8: Battery Comparison: XINJ 102540 vs Higher Capacity Batteries

Parameters	XINJ 102540 (1300mAh)	Battery 2 (2000mAh)	Battery 3 (3000mAh)
Nominal Voltage	3.7V	3.7V	3.7V
Charge Current	1A	1.5A	2A
Capacity	1300mAh	2000mAh	3000mAh
Energy	4.81mWh	7.4mWh	11.1mWh
Size (Length)	4.0 cm	5.0 cm	6.0 cm
Size (Width)	2.5 cm	3.0 cm	3.5 cm
Size (Thickness)	1.0 cm	1.2 cm	1.5 cm
Protection Circuit	Yes	Yes	Yes

Additionally, this battery features an integrated protection circuit, which makes the power stage more robust by protecting against overloads and any potential issues related to the USB bus.

3.9 Battery Charger

As the device is used continuously, it was necessary to choose a rechargeable battery. The MCP73831 was used as the driver to recharge the XINJ 102540 battery. The main parameters considered were the charging voltage, the charging current, and the input voltage. It was optimal for the charging current to be 1A, as it was the maximum the battery could handle, making it unnecessary to choose a component with a higher current rating. All other parameters were also selected based on the battery. This controller proved to be the right choice for this circuit, as other components were more expensive and did not offer significant advantages due to the limitations of the chosen battery.

Table 9: Comparison of Li-Ion/Li-Polymer Battery Charger ICs

Parameters	MCP73831	TP4056	MCP73871
Input Voltage	3.75V to 6.0V	4.5V to 5.5V	4.5V to 6.0V
Charge Voltage	4.2V	4.2V	4.2V
Charge Current	1A (typical)	2A (typical)	1A (typical)
Charge Current Regulation	1%	1%	1%
Standby Current	30µA (typical)	2µA (typical)	30µA (typical)
Charge Termination Current	50mA (typical)	50mA (typical)	50mA (typical)
Thermal Regulation	125°C	125°C	125°C
Package Type	SOT-23	SOP-8	QFN-16
Operating Temperature Range	-40°C to +85°C	-40°C to +85°C	-40°C to +85°C

3.10 Voltage Regulator

The choice of LDO is probably the most important among power ICs, as it defines the bias voltage for the entire circuit and the maximum current the circuit can draw. Considering that the ESP32

should not consume more than 250mA when using the Wi-Fi module and that it represents almost all the circuit's consumption, the MIC5504-3.3YM5 was selected, as it has a maximum output current of 300mA. It was also decided that the voltage that would power the entire circuit would be 3.3V, as it was noted that there was no need for 5V or higher for either the digital part or the amplifiers, which allowed for the use of a lower voltage battery.

Table 10: Comparison of LDO Regulators: MIC5504-3.3YM5 vs Other LDOs

Parameters	MIC5504-3.3YM5	AMS1117-3.3	LD1117-3.3
Output Voltage	3.3V	3.3V	3.3V
Output Current	300mA (max)	800mA (max)	800mA (max)
Dropout Voltage	40mV @ 150mA	1.1V @ 800mA	1.1V @ 800mA
Input Voltage Range	1.8V to 5.5V	4.75V to 15V	4.75V to 15V
Quiescent Current	35µA (typ)	5mA (typ)	5mA (typ)
Package Type	SOT-23-5	TO-220	TO-220
Operating Temperature Range	-40°C to +125°C	0°C to +125°C	0°C to +125°C

Another important advantage of this voltage regulator is that it has an enable pin, which is used to power off the circuit through the ESP32. When the LDO is disabled, the entire power supply, including the negative voltage for the digital part, does not receive energy, ensuring that the battery does not discharge in this mode.

3.11 USB Port

A USB port needed to be chosen to supply the power to the battery. It was decided that the port would be USB-C, as it is currently the most common and modern connector available. Additionally, it can supply more power and current than USB 2.0, and is significantly smaller than these. Micro USB was considered, as it is less powerful, but it is now largely obsolete. Therefore, it was deemed best to use USB-C, even though its full potential would not be fully utilized.

Table 11: Comparison of USB-C, Micro USB, and USB 2.0 for Power Transmission

Parameters	USB-C	Micro USB	USB 2.0
Maximum Power (W)	100W	18W	2.5W
Voltage	5V, 9V	5V	5V
Current	Up to 5A	1.5A	0.5A
Power Delivery (PD)	Yes (Supports PD)	No	No
Connector Reversibility	Yes	No	No

3.12 Negative Voltage Regulator

Since the digital logic of the circuit was designed with PMOS transistors, it was necessary to have a -3.3V power supply to properly bias the transistors when required by the logic. To achieve this, the TC7662B was selected, as it converts the 3.3V output from the LDO to -3.3V. When choosing this component, the focus was on selecting a DC-DC converter with good efficiency and minimal noise. A high output current was not necessary because this voltage would only be used in the digital part of the system, where static power consumption is close to zero.

Table 12: Comparison of Voltage Inverters: TC7662B vs ICL7660 vs MAX232

Parameters	**TC7662B**	**ICL7660**	**MAX232**
Voltage Conversion	3.3V to -3.3V	5V to -5V	3.3V to -12V
Maximum Output Voltage	-3.3V	-5V	-12V
Output Current (max)	20mA	10mA	8mA
Efficiency	75% (typical)	70% (typical)	50% (typical)
Package Type	8-pin SOIC	8-pin SOIC	16-pin DIP
Operating Temperature Range	-40°C to +125°C	-40°C to +85°C	0°C to +70°C

4 Data Transmission

To achieve real-time, wireless transmission of current measurements from the ESP32 to a remote interface, the WebSocket protocol was selected for this project. WebSockets offer a full-duplex communication channel over a single TCP connection, making them ideal for applications that require continuous, low-latency data exchange between a client and a server.
In this implementation, the ESP32 acts as the WebSocket server, hosting a connection on port 81. The webpage, accessed via a browser on a computer or smartphone, functions as the WebSocket client. Once connected, the client remains open for the duration of the session, allowing the ESP32 to transmit current measurements instantly as they are acquired. For more details about the code, check Appendix 9.

This protocol was chosen over alternatives such as HTTP polling or MQTT for several reasons:

- Low latency: WebSockets eliminate the overhead of repeated HTTP requests, enabling faster data updates, which is critical for visualizing dynamic current changes.
- Simplicity of integration: WebSockets are natively supported in modern web browsers, allowing seamless integration with a lightweight HTML/JavaScript-based user interface.
- Bi-directional communication: Although not currently used in this project, the WebSocket infrastructure allows future expansions where control commands (e.g., start/stop measurement, change display settings) could be sent from the client to the ESP32.

Overall, the use of WebSocket communication aligns with the project's goals of real-time monitoring, platform independence, and efficient wireless operation, without requiring additional middleware or complex networking stacks. Fig. 2 shows the website created to show the measured data in real time from a cellphone or a computer:

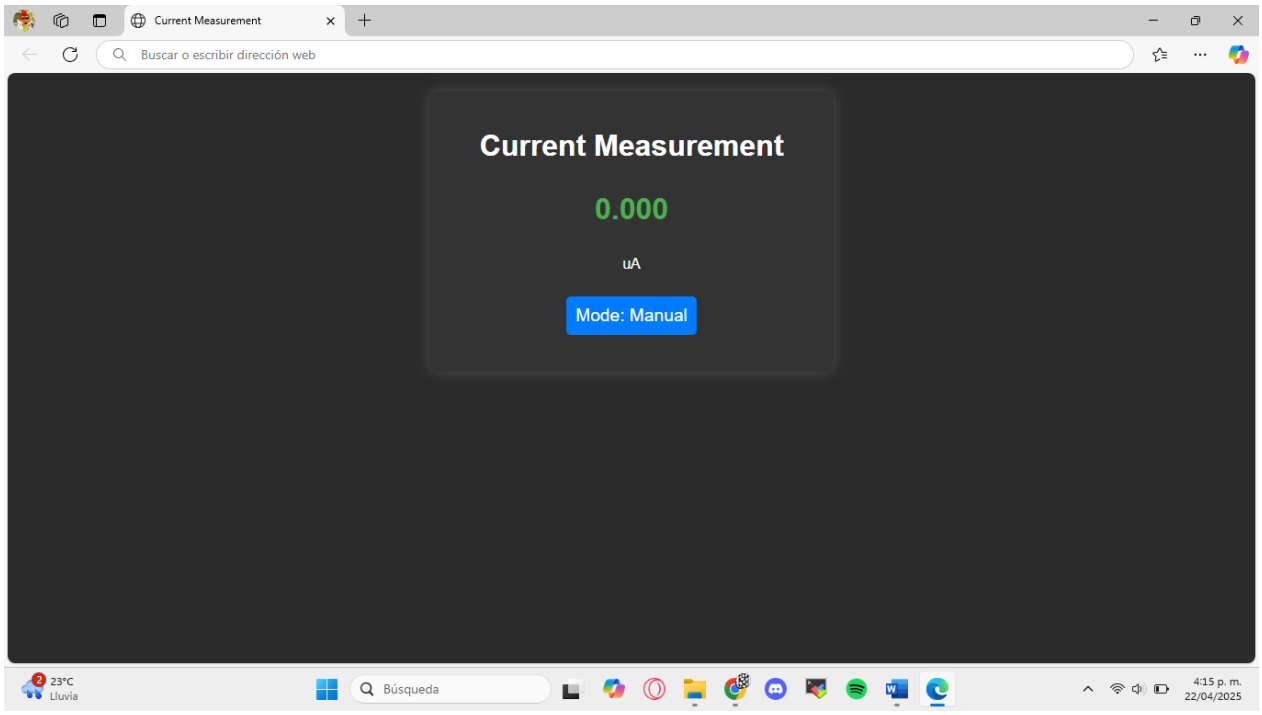

Figure 2: Website used to receive current measurements.

5 Simulation Analysis

5.1 Nominal Simulation

The simulation software chosen to carry out this task was LTspice by Analog Devices [3]. This software was selected because, in addition to being open-source, it is one of the most versatile tools for circuit simulation. Its analysis features and user-friendly interface make it highly suitable for running complex simulations, such as Monte Carlo simulations. Although the entire circuit was analyzed to fully understand its operation, it was decided to simulate only the core of the circuit, which consists of the logic implemented with transistors and the subsequent amplification stage. VDD and VNEG were simulated as two ideal voltage sources, just like the digital signals.

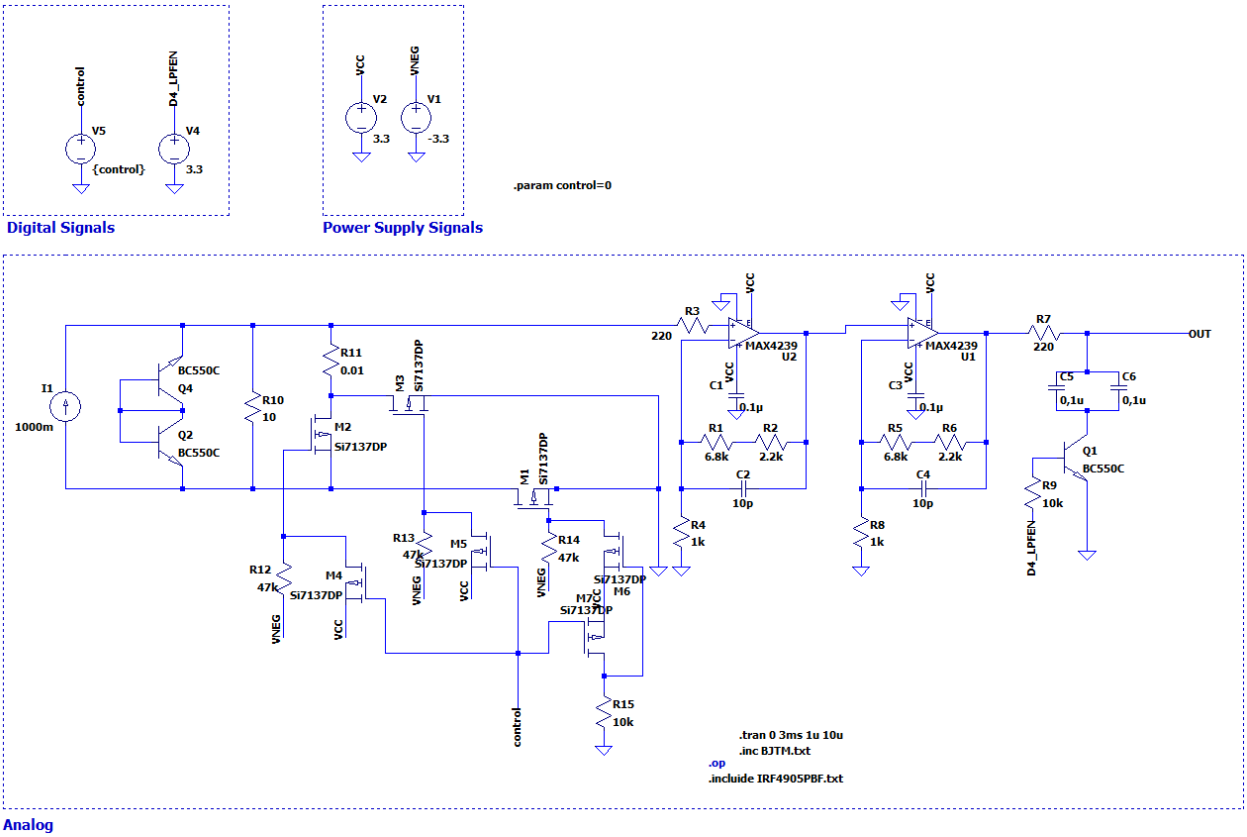

Figure 3: Simulation Schematic

The input signal was modeled as an ideal current source, and the simulation focuses on verifying the logic of the PMOS transistors and obtaining the desired output voltage through the amplifiers. It is important to clarify that all devices in this simulation, except for the resistors and capacitors, are real devices, meaning that undesirable side effects such as bias currents, offset in the amplifiers, and parasitic capacitances in the PMOS transistors are already accounted for. The resistors and capacitors will undergo their respective analysis when the Monte Carlo analysis is performed.

The setup used for the nominal simulation was as follows:

Although the circuit is completely DC, a transient simulation was performed from 0 to 3ms with a step of 1µs in order to observe and verify that there were no peaks or distortions in both the input and output signals during the transient response. Additionally, it was necessary to include the models of both the BJTs used and the PMOS transistors.

Table 13: Simulation Setup Information

Command	Description	File Reference
`.tran 0 3ms 1u 10u`	Transient simulation parameters	N/A
`.inc BJTM.txt`	Include BJTM model file	BJTM.txt
`.include IRF4905PBF.txt`	Include IRF4905PBF model file	IRF4905PBF.txt

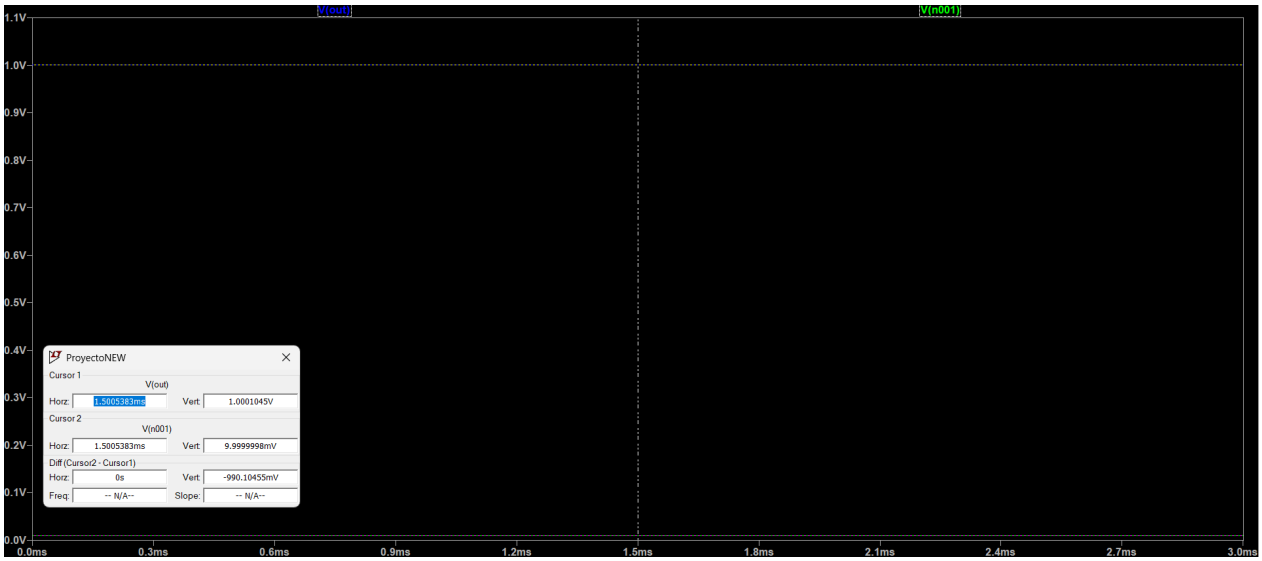

Figure 4: A transient simulation was performed in microcurrent mode with a current of I = 1000µA.

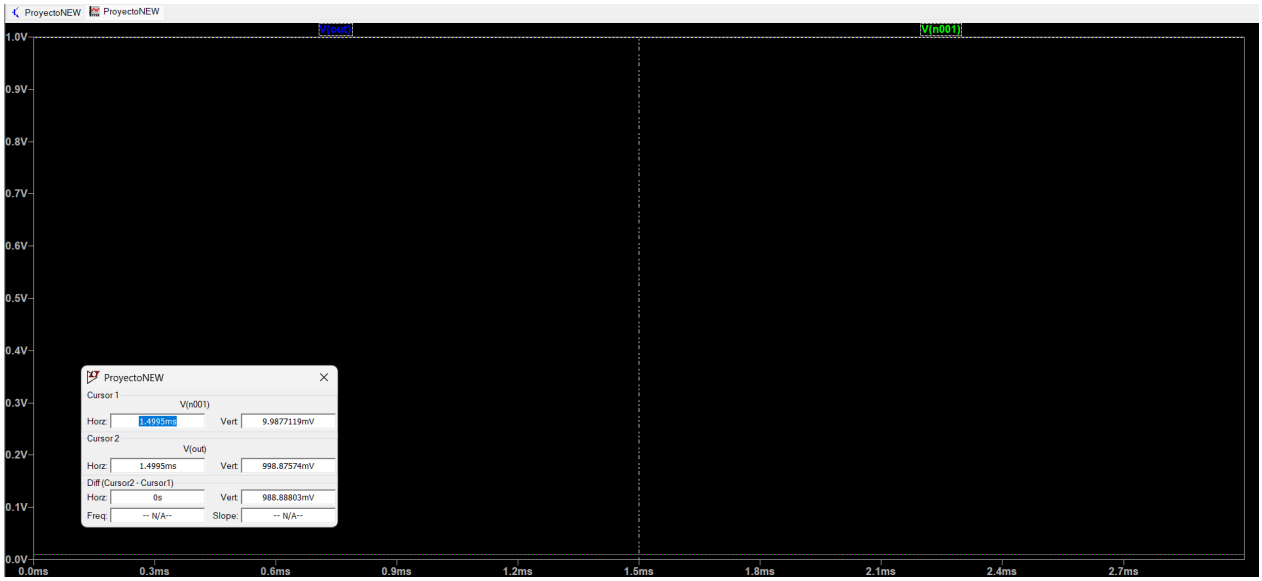

Figure 5: A transient simulation was performed in milicurrent mode with a current of I = 1000mA.

In the nominal simulation, the expected results were obtained. The output voltage range varied from 1mV to 1V for both modes of operation, thanks to the difference in the values of the SHUNT resistors. In the milicurrent mode, a 0.11% error was observed in its nominal operation. For the application considered, this error is entirely acceptable and is due to the unwanted effects of the components in the circuit.

Table 14: Simulation Values and Error Percentage

	Vout (V)	**Vn001 (V)**	**% Error Vout**
MicroCurrent	1.0001045	0.0099999998	0.0104
MiliCurrent	0.99887574	0.0099877119	0.1124

5.2 Monte-Carlo Simulation

Previously, a nominal simulation was performed, which included secondary effects such as offset but did not account for other real-world factors like resistor tolerance—that is, the fact that actual resistors rarely match their nominal values exactly. To address this limitation, a Monte Carlo simulation was conducted. This approach introduces variations not only in resistor values but also in capacitances and the supply voltage (VCC), aiming to capture worst-case scenarios in the circuit's performance.

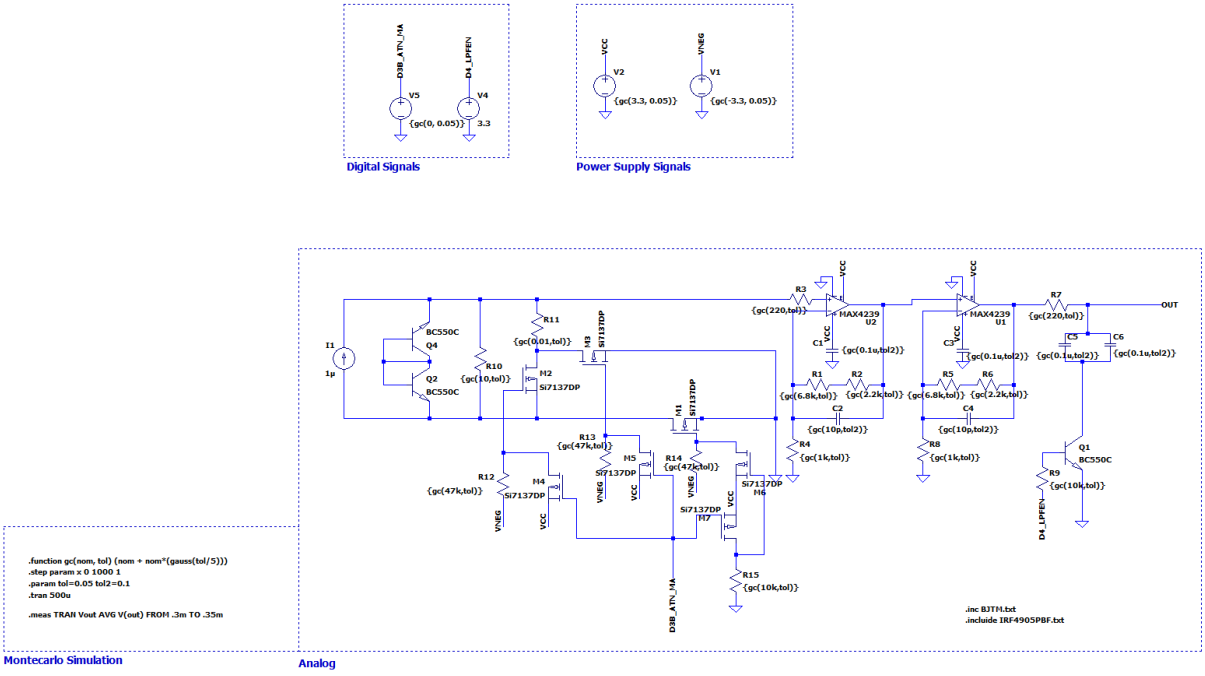

Figure 6: Simulation Schematic

To perform the Monte Carlo test, we based our approach on the documentation provided by Analog Devices, where we first defined a Gaussian distribution, which we would run 1,000 times. We defined a 5% tolerance, which is considered quite high for all components, in order to account for the worst-case scenarios. Finally, a transient test is performed, and data is extracted at a given time, which, since it is a DC circuit, makes the time selection irrelevant.

Table 15: Simulation Setup Information

Command	Description
`.function gc(nom, tol) (nom + nom*(gauss(tol/5)))`	Gaussian distribution function
`.step param x 0 1000 1`	Step through parameter x
`.param tol=0.05 tol2=0.1`	Set parameters for tolerance
`.tran 500u`	Transient simulation for 500µs
`.meas TRAN Vout AVG V(out) FROM 3m TO 35m`	Measure transient output voltage from 3ms to 35ms

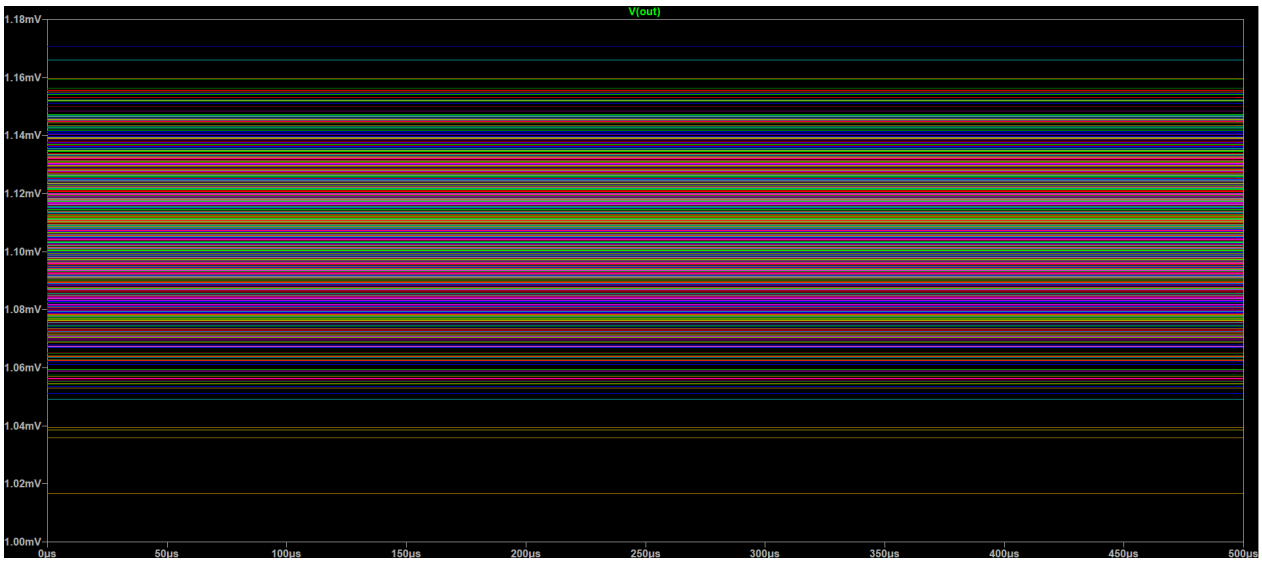

Figure 7: Simulation Results

Subsequently, data extraction is performed through LTspice and then transferred to a Python environment for further data analysis, enabling the extraction of curves and values of interest.

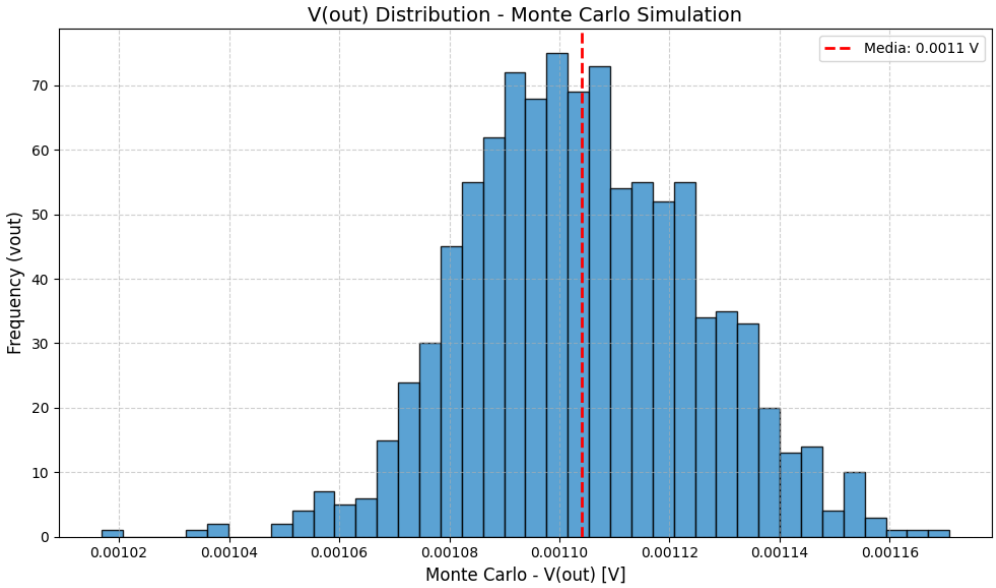

Figure 8: Output Distribution

Thanks to the extracted distribution, we can obtain the following statistical data, which will be necessary to analyze the results.

Table 16: Statistical Data from Monte Carlo Simulation

Statistic	**Value (V)**
Mean	0.001104
Median	0.001103
Standard deviation σ	0.000021
Variance	0.000000
Minimum	0.001017
Maximum	0.001171

Finally, a basic analysis is conducted in which we state that the 3-sigma rule ensures that 99.73% of the data falls within the statistical distribution. Therefore, this calculation was performed using the mean as the starting point to determine the worst-case scenarios under a Gaussian distribution. The results showed that the lower limit yielded a 4% error, indicating that the circuit does not tend to vary downward under Monte Carlo variations. In contrast, the upper limit resulted in a 16% error, suggesting that the majority of the deviation is concentrated in that region. Despite being a relatively high error, we do not consider it to be highly significant, as it must be noted that the component variations used in the simulation were greater than what would typically be expected. In the actual implementation, this deviation should be considerably lower.

Table 17: Calculation of the 3σ Range Around the Mean

Description	**Value (V)**
3σ	0.000063
Lower bound (Mean -3σ)	0.001041
Upper bound (Mean $+3\sigma$)	0.001167
Expected range ($\pm 3\sigma$)	0.001041 – 0.001167
Relative error from ideal (0.001V)	Lower: 4.1%, Upper: 16.7%

To conclude, the same analysis was carried out using the MiliCurrent mode with an input current of I = 1000mA, and the following results were obtained:

Table 18: Calculation of the 3σ Range Around the Mean (MiliCurrent Mode, $I = 1000$mA)

Description	**Value (V)**
3σ	0.059004
Lower bound (Mean -3σ)	0.939027
Upper bound (Mean $+3\sigma$)	1.057035
Expected range ($\pm 3\sigma$)	0.939027 – 1.057035
Relative error from ideal (1.000V)	Lower: 6.10%, Upper: 5.70%

6 PCB design

6.1 Schematic

After carefully selecting the components, the assembly is carried out in KiCad 9.0 software, which contains the necessary tools to create the PCB. The schematic is developed by combining the two most important parts: the analog circuit itself and its corresponding power section. Additionally, a method of interacting with the user was implemented through 5 LEDs, which provide relevant information regarding the device's charge, power status, and operating mode. At this stage, the selection of components for user interaction was also completed, such as the screw terminal for input current and the footprints of each element, all appropriately chosen.

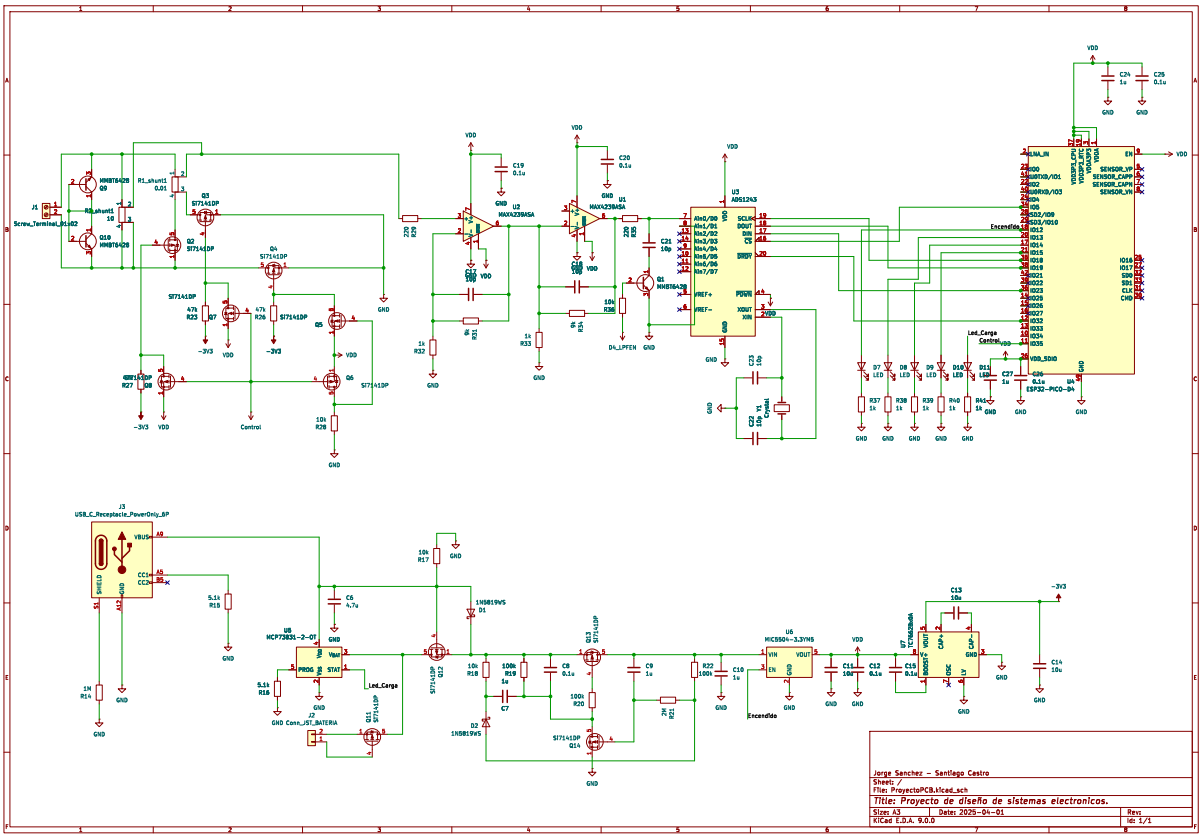

Figure 9: Schematic of the Complete Project

After selecting the components, the operational diagrams of each integrated circuit in the power stage were researched to later apply them and ensure their proper functioning. It was checked that no floating nodes remained in order to avoid issues when designing the PCB.

6.2 PCB Layout

The PCB layout faced several challenges, among which placement and routing stand out. First, the board size was defined in such a way that the components would not overlap. After conducting this analysis, the chosen area was 64.5x49 [mm^2], where it was demonstrated that all elements could be placed correctly. Subsequently, the placement of each component was carried out, considering the proximity of components to each other and the need for central placement. Additionally, the layout was made intuitive for the user, such as the positioning of the USB-C port and the screw terminal for input current, which facilitates ease of use.

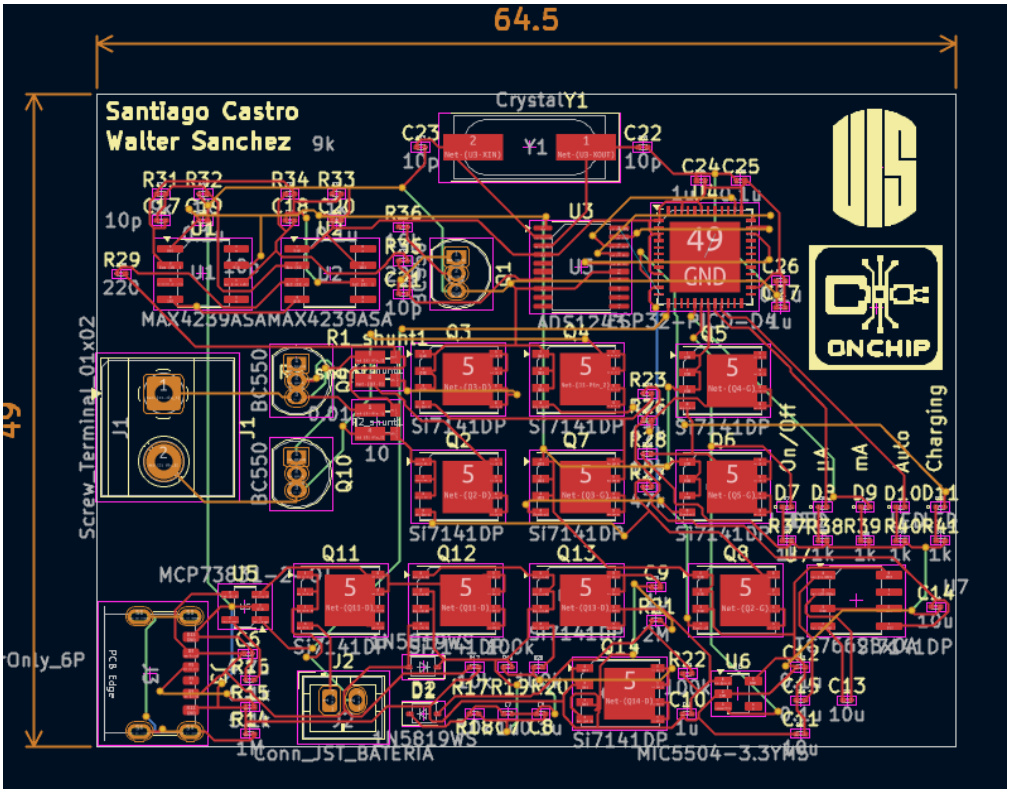

Figure 10: Layout of the PCB

When performing the PCB routing, it was decided to use 4 layers due to the limited space, which made it impossible to complete all the vias on a single layer. In the layout image, the four layers can be identified, which consist of two outer layers and two inner layers, distinguished by the colors red, blue, green, and orange. Thanks to this approach, the PCB was made with a significantly small size. Finally, the protoboard was customized by incorporating the identity of the UIS and our research group, and labels were added to identify each LED with its respective function.

The final result of the PCB with its 3D model is as follows:

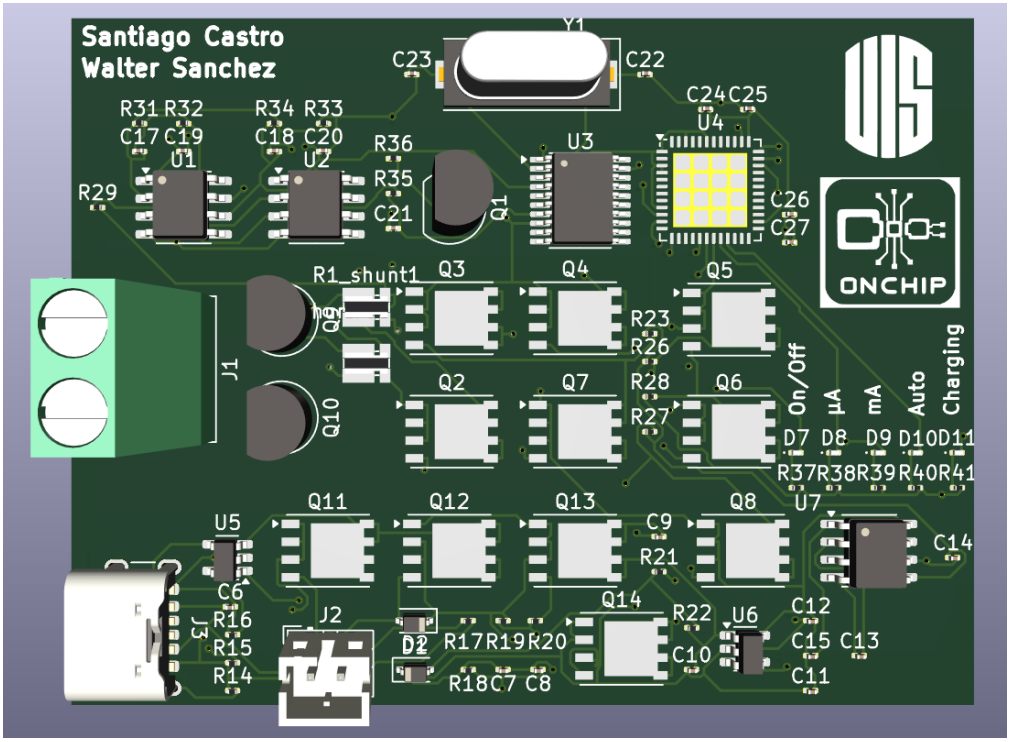

Figure 11: Final 3D Model

6.3 PCB Revision and Improvements

Once the PCB was completed, a thorough study was carried out to identify areas for improvement. It was concluded that there were key components whose placement could have been better, such as the ESP32 chip and the LDO. The former controls a large part of the circuit, so it has many associated connections, while the latter provides the bias voltages for the entire circuit. Therefore, these components could be positioned more centrally. Although, in general, the circuit does not carry excessively large currents, the layout could also be resized to accommodate larger vias depending on the amount of current flowing through them, especially in the case of the ESP32.

Thermal analysis could also be performed to ensure there are no overheating issues in the circuit. This is done using heat maps that evaluate which parts of the PCB are most affected by the thermal energy dissipated by the electronic components. Finally, it is necessary to thoroughly review the DRC (Design Rule Check) regulations to confirm that there will be no issues when implementing the PCB.

7 Cost Estimation

Table 19: Bill of Materials with Estimated Unit Prices

Component	**Reference**	**Value**	**Quantity**	**Unit Price (USD)**
Battery	XINJ 102540	3.7V	1	5.00
Resistor	N/A	10kΩ	4	0.01
Resistor	N/A	9kΩ	2	0.01
Resistor	N/A	1kΩ	7	0.01
Resistor	N/A	47kΩ	3	0.01
Resistor	N/A	220Ω	2	0.01
Resistor	N/A	100kΩ	3	0.01
Resistor	N/A	5.1kΩ	2	0.01
Resistor	N/A	1MΩ	1	0.01
Resistor	N/A	10Ω	1	0.01
Resistor	N/A	2MΩ	1	0.01
Shunt Resistor	N/A	0.01Ω	1	0.10
Shunt Resistor	N/A	10Ω	1	0.10
Capacitor	N/A	4.7µF	1	0.02
Capacitor	N/A	1µF	5	0.02
Capacitor	N/A	0.1µF	7	0.02
Capacitor	N/A	10µF	3	0.02
Capacitor	N/A	10pF	5	0.02
Diode	N/A	N/A	2	0.05
PMOS Transistor	Si7141DP	N/A	11	0.50
BJT Transistor	BC550	N/A	1	0.10
BJT Transistor	MMBT6429	N/A	1	0.10
BJT Transistor	MMBT6428	N/A	1	0.10
Op-Amp	MAX4239	N/A	2	2.00
ADC	ADS1242IPWT-1	N/A	1	8.00
Microcontroller	ESP32-WROOM-32E	N/A	1	3.00
LED Diode	N/A	N/A	5	0.05
Crystal	ABLS2	N/A	1	0.20
Battery Charger	MCP73831	N/A	1	0.50
Voltage Regulator	MIC5504-3.3YM5	N/A	1	0.20
Negative Voltage Regulator	TC7662B	N/A	1	1.50
USB-C Port	N/A	N/A	1	0.50
Screw Terminal	N/A	N/A	2	0.20
Total Cost				**$30.00**

8 Conclusions

- The power circuit was designed to supply the entire system from 3 key chips: MCP7383, MIC5504, and TC7662B, which were selected based on the current and voltage requirements of the circuit. If the nominal supply voltage needs to be changed or if additional components that significantly increase current consumption are added, it will be necessary to re-evaluate the selected components to ensure they meet the new specifications. The chosen battery ensures a 2-hour daily operation on a weekly basis, aiming for a small and lightweight device. On the other hand, higher capacity would have complicated the PCB design process and its subsequent use.

- The results of the nominal simulation show that the achieved error is completely acceptable, ranging from 0.0104% to 0.1124%. We can conclude that this device will operate with a significantly high precision and will be able to measure within the selected ranges with up to 3 decimal places of accuracy, which is more than acceptable for a wide range of applications. The error is generated by secondary effects such as offset and bias currents, as well as parasitic resistances and capacitances produced by the transistors used in the circuit's logic. Therefore, if a lower error is required, it is essential to reconsider all the components, especially the operational amplifiers.

- In the Monte Carlo simulation, excessively high tolerances were purposely chosen to consider components that were not highly precise. Even though resistors and capacitors typically have much lower tolerances, this simulation presents a pessimistic view of the circuit's behavior through variations. Despite this, the worst error achieved was 16% for the microcurrent mode, which we consider to be a very small error, as the probability of it occurring is less than 0.7%. It is concluded that the built circuit is robust against such variations. The distribution used to model these changes was the Gaussian distribution, as it is present in many natural phenomena, such as variations in resistance. Additionally, the bias source was varied by 5% to observe and demonstrate what could happen if the LDO does not provide the exact 3.3V. Even so, the circuit operates correctly with relatively low errors.

- The cost estimation for the fully assembled board indicates that the implementation of the proposed system is relatively low. This is particularly notable given the device's high-precision performance requirements. The selected components, including the precision ADC, low-noise operational amplifiers, and the ESP32 microcontroller, contribute to achieving accurate and reliable measurements while maintaining a cost-effective design. Therefore, the proposed solution offers a promising balance between performance and affordability, making it suitable for scalable applications in both research and industry.

References

[1] LowPowerLab, "Low-pass filter function (lpf)," 2025. Accessed: Mar. 30, 2025.

[2] F. Rusu, "Currentranger – ultra low power current measurement." https://lowpowerlab.com/guide/currentranger/, 2018. Accessed: 2025-04-23.

[3] Linear Technology, *LTspice IV Getting Started Guide*. Linear Technology, 2011. Available as PDF presentation: Microsoft PowerPoint - LTspiceGettingStartedGuide.ppt.

9 Appendix

9.1 GitHub Repository

The source code and design files related to this project are available in the following public GitHub repository:

- `Current_Meter` – https://github.com/Scastrx/Current_Meter

This repository includes firmware, schematics, and documentation essential for reproducing or modifying the current measurement system.